Generation of All-focus Images and Depth-adjustable Images Based on Pixel Blurriness

Yi-Chong Zeng
Advanced Research Institute, Institute for Information Industry, Taipei, Taiwan, R.O.C.
E-mail: yichongzeng@iii.org.tw Tel:+886-2-66072958

***Abstract*—Taking a picture containing all-focus objects with regardless of distance is difficult. A feasible strategy to generate an all-focus image relies on multiple images with different focus settings. Furthermore, image refocusing with side information is applied to all-focus image to generate depth-adjustable image which is like to real-world photos at the specified depth-of-field. In this paper, we propose image fusion and refocusing methods for generation of all-focus image and depth-adjustable image. During fusion procedure, measuring pixels' blurriness of multi-focus reference images is the first process. Then, all-focus image composed of sharpest pixels among reference images, index map, and standard deviation-index table are yielded. The objective of standard deviation-index table is to connect relationship between Gaussian lowpass filter and index. During refocusing procedure, different Gaussian lowpass filters applied to all-focus image by referring to index map and standard deviation-index table, and then depth-adjustable image is generated. The experiment results demonstrate the proposed methods are better than the compared approaches in computational complexity and quality of all-focus image and depth-adjustable image.**

I. INTRODUCTION

Digital camera becomes popular and has been integrated into many electronic products, such as mobile phone, notebook, and tablet. The big challenge for photography is to take a picture containing all objects in focus with regardless of distance. Due to digital camera takes a picture with a fixed focus setting, object within the specified depth of field is taken in focus, the rest of objects are out of focus and become blurry. In 2006, Ng's Ph.D thesis [1] put forward a theory to acquire all-focus image by digital light field photography. In 2011, Lytro Inc. developed a consumer light-field digital camera which acquired images using plenoptic technique. However, low resolution is the major drawback to such products.

In order to generate image containing all objects in focus, an easy way is realized by fusing multi-focus images. There were hugely numerical literatures to investigate image fusion. Naidu published so many literatures with respect to image fusion, his approaches were implemented by fast Fourier transform (FFT) [2], discrete cosine transform (DCT) [3], principal component analysis (PCA) [4], singular value decomposition (SVD) [5], dual tree complex wavelet transform (DT-CWT) [6], and etc. In [7, 8, 9], the researchers used neural network to implement image fusion, such as Li et al. used artificial neural network [7], Huang et al. [8] and Qu et al. [9] employed pulse coupled neural network (PCNN). Spatial based fusion methods had been addressed in [10-12]. In [13], Kong et al. integrated genetic algorithm with spatial frequency information. Furthermore, wavelet-based fusion approaches had been introduced in [14-17].

Contrary to image fusion, the objective of image refocusing is to generate image with different depth of fields. In the generic framework, depth or depth-blurriness information is essential for image refocusing. In [18], Bae and Durand estimated the spatially-varying amount of blur as well as the size of blur kernel at edges, and then magnified blurring effect in blurry regions but kept sharpness of sharp regions. In [19], Moreno-Noguer et al. proposed a system to refocus images and videos. They acquired depth information based on the defocus of a sparse set of dots projected onto the scene. Subsequently, alpha-map with respect to depth information was matted with two refocused images to generate final refocused image.

In this paper, we propose two methods, namely image fusion and image refocusing, to generate all-focus image and depth-adjustable image. Pixel blurriness measure is the key, which is a criterion to distinguish blurry pixels from sharp ones. Pixel blurriness is computed based on variation of intensity differences. Intensity difference is defined as the difference between two blurred images which are derived from the same original image smoothed by two different Gaussian lowpass filters. During fusion procedure, our method collects all sharpest pixels among multi-focus reference images and forms an all-focus image. Meanwhile, an index map, consists of indices of sharpest pixels derived from which reference images are, is produced. Afterward, analyzing the relationship between Gaussian lowpass filter and image index conducts to establish standard deviation-index table. During refocusing procedure, different Gaussian lowpass filters are applied to all-focus image by referring to index map and standard deviation-index table, and then depth-adjustable image with the specified index/depth is generated. Under certain circumstance, the proposed fusion method is one kind of image enhancement, this work can be applied to video surveillance application for improvement of video content. The rest of this paper is organized as follows: Section II will briefly introduce pixel blurriness measure. The proposed image fusion method and image refocusing method will be introduced in Sections III and IV, respectively. The experiment results will be shown in Section V, and the concluding remarks will be drawn in Section VI.

II. PIXEL BLURRINESS MEASURE

In the previous work [20], we proposed a method to measure pixel blurriness, and used it to detect salient objects in image and video. The pixel blurriness is computed based on variation of high-frequency energy within the specified region. Generally speaking, sharp region (intense-variant signal) has more details than blurry region (moderate-variant signal) does. High-frequency energy highly associates with detail of region. Therefore, high-frequency energy in sharp region is larger than that in blurry region, which is verified in [20]. Once blurry region and sharp region are smoothed by lowpass filter, sharp region loses more high-frequency energy than blurry region does. Summarizing the above descriptions, *the pixel blurriness is defined as variation of high-frequency energy to the target image processed with various blurriness degrees of lowpass filters*.

The steps of pixel blurriness measure are described below. In the first step, multiple lowpass filters are applied to target image, which is given by,

$$\mathrm{I}_k = \mathrm{I}_0 \otimes \Phi_k, \tag{1}$$

where I_0 is the intensity of target image, I_k is the smooth result of I_0 operated with the k-th lowpass filter Φ_k and $\|\Phi_k\|_1=1$. The symbol '$\otimes$' is the convolution operator. The Φ_k must make image blurrier than the Φ_{k-1} does. Subsequently, the difference between two smooth images is computed,

$$\Psi_k(x,y)=\sum_{i=-L}^{L}\sum_{j=-L}^{L}\left|I_{k-1}(x+i,y+j)-I_k(x+i,y+j)\right|^2, \tag{2}$$

where $\Psi_k(x,y)$ denotes the (x,y)-th pixel value in the k-th difference image, and L is the half height/width of the selected region. As we mentioned before, large difference means that region loses more high-frequency energy after lowpass filtering. The pixel with the largest difference represents that it is sharpest among all pixels. Four difference images are sufficient to compute variation of intensity difference (VID). The VID is the slope of a straight line which approximates to four difference values (denoted as $\Psi_1(x,y)$, $\Psi_2(x,y)$, $\Psi_3(x,y)$ and $\Psi_4(x,y)$), and it is formulated as below,

$$\begin{aligned} s(x,y) &= \frac{-\sum_{k=1}^{4}k\cdot\sum_{k=1}^{4}\Psi_k(x,y)+4\sum_{k=1}^{4}k\cdot\Psi_k(x,y)}{4\sum_{k=1}^{4}k^2-\left(\sum_{k=1}^{4}k\right)^2} \\ &= -0.3\cdot\Psi_1(x,y)-0.1\cdot\Psi_2(x,y)+0.1\cdot\Psi_3(x,y)+0.3\cdot\Psi_4(x,y) \end{aligned} \tag{3}$$

In (3), $s(x,y)$ denotes the slop of the approximate line as well as pixel blurriness of the (x,y)-th pixel. The VID is robust to illumination changing. Assuming that illumination changing occurs at a small region of sized $(2L+1)\times(2L+1)$, pixel with influence of illumination changing is defined as $\tilde{I}_0(x,y)= I_0(x,y)+c$, where c is an intensity offset as well as a constant. The difference between two smooth images is rewritten to,

$$\begin{aligned} \Psi_k(x,y) &= \sum_{i=-L}^{L}\sum_{j=-L}^{L}\left|\tilde{I}_{k-1}(x+i,y+j)-\tilde{I}_k(x+i,y+j)\right|^2 \\ &= \sum_{i=-L}^{L}\sum_{j=-L}^{L}\left|I_{k-1}(x+i,y+j)-I_k(x+i,y+j)\right|^2 \end{aligned} \tag{4}$$

where $\tilde{\mathrm{I}}_k = \tilde{\mathrm{I}}_0 \otimes \Phi_k = (\mathrm{I}_0 + c)\otimes\Phi_k = \mathrm{I}_0\otimes\Phi_k + c$

(a) (b)

Fig.1. Edge Inconsistency: (a) the all-focus image, and (b) the enlargement of inconsistent edges of region

Comparing (2) and (4), it is obvious that pixel blurriness measure is invariant to illumination changing in small region.

III. IMAGE FUSION METHOD

In our assumption, all-focus image consists of sharpest pixels among multi-focus reference images. Assuming that the (x,y)-th sharpest pixel in the k^*-th reference image has smallest pixel blurriness than those in the rest of reference images, which is defined as follows:

$$\begin{aligned} &\hat{I}(x,y) = I_{k^*}(x,y), \\ &\text{where } k^* = \underset{k\in\{1,2,\ldots,N_{\mathrm{ref}}\}}{\arg\min}\ s_k(x,y). \end{aligned} \tag{5}$$

In (5), $\hat{I}(x,y)$ and $I_{k^*}(x,y)$ denote the (x,y)-th pixel values of the all-focus image and the k^*-th reference image, respectively. N_{ref} is the number of reference images. However, this way gives rise to a problem of edge inconsistency. Fig.1(a) is the all-focus image generated by using the above-mentioned method. However, the inconsistent edges appear at the margin of paper cup, and the enlargement is shown in Fig.1(b). The proposed fusion method is composed of three procedures: pixel blurriness measure, classification of blurry and sharp pixels, and generation of all-focus image. The detail of every procedure is introduced below.

A. Pixel Blurriness Measure

Section II has introduced the processes to measure pixel blurriness. In [20], average filter with different sizes (such as 7×7, 11×11, 15×15, and 19×19) was employed as lowpass filters. In this work, we use Gaussian lowpass filter instead of average filter. Gaussian lowpass filter has higher association with human vision system than average filter does. When eyes focus on an object, the surroundings of object are blurry. In [21], McAnany et al. addressed that the intrinsic blur is Gaussian in nature. They characterized optical blur by the Gaussian functions to fit to the point spread functions (PSFs). Therefore, Gaussian lowpass filters with four standard deviations σ_i apply to target image, where $\sigma_1 < \sigma_2 < \sigma_3 < \sigma_4$. We assume that the four blurred results are similar to optical blur in visual acuity. In the experiments, the Gaussian lowpass filter is sized to 23×23, and the standard deviations are set to σ_1=0.1, σ_2=5, σ_3=10, and σ_4=20.

B. *Classification of Blurry, Bordered and Sharp Pixels*

Analyzing inconsistent edge, it almost appears at smooth region or boundary between smooth and sharp regions. In order to prevent inconsistent edges, the strategy of using different approaches deals with sharp pixel, blurry pixel, and bordered pixel. The first work is to classify pixel into three classes. Let Ω_j be the j-th intensity block of sized 23×23, and s_j be the pixel blurriness of the center pixel in Ω_j. Fig.2(a) shows three blocks composed of three kinds of pixels, and the Gaussian distributions of pixel blurriness to sharp pixels, bordered pixels, and blurry pixels are drawn in Fig.2(b). The figure depicts that blurry pixel has larger pixel blurriness than sharp pixel and bordered pixel do. In addition, the Gaussian distributions of sharp pixel and bordered pixel are very close to each other.

In [22, 23], the discriminant function $q(s)$ was proposed to classify two distributions, such as g_1 and g_2, which is formulated as,

$$q(s)=\ln\frac{p(s\,|\,g_1)}{p(s\,|\,g_2)}+\ln\frac{p(g_1)}{p(g_2)} \tag{6}$$

where s is defined as the pixel blurriness. The notations $p(g_i)$ and $p(s|g_i)$ denote the probability of g_i and the conditional probability of s when g_i is given, respectively. Subsequently, the threshold classifies two distributions is defined as,

$$\tau=\underset{T_1<s<T_2}{\operatorname{argmin}}\left|q(s)\right|, \tag{7}$$

where the threshold τ is estimated between two limits, T_1 and T_2. For the case of Fig.2, the threshold between blurry pixel and non-blurred pixel is τ_1=–0.7166, and the threshold between sharp pixel and bordered pixel is τ_2=–1.3629. Thus, the discriminant criterion of pixel classification is defined as,

$$\Theta(x,y)=\begin{cases}1, & \text{if } s(x,y)\ge\tau_1,\\ 0, & \text{if } \tau_2\le s(x,y)<\tau_1,\\ -1, & \text{otherwise}\end{cases} \tag{8}$$

where $\Theta(x,y)$ represents the pixel class of the (x,y)-th pixel. If $\Theta(x,y)$=1, the pixel is identified as blurry pixel; if $\Theta(x,y)$=0, the pixel is identified as bordered pixel; if $\Theta(x,y)$=–1, the pixel is identified as sharp pixel.

C. *Generation of All-focus Image*

The steps of generation of all-focus image are described below.

Step 1. Assuming that all multi-focus reference images are rearranged from the short-distant image to the long-distant image. $\hat{\mathrm{I}}$ and I_j denote the all-focus image and the j-th reference image, respectively. The notation Θ is the pixels' class image of $\hat{\mathrm{I}}$. Let τ_1 and τ_2 be two thresholds to pixel classification. An example is shown in Fig.3.

Step 2. Picking up all sharpest pixels among reference images, those pixels form $\hat{\mathrm{I}}$ by (5). Meanwhile, the index map (denoted as Λ) composed of the indices of sharpest pixels derive from which reference images are, is produced and defined as $\Lambda(x,y)=k^*$.

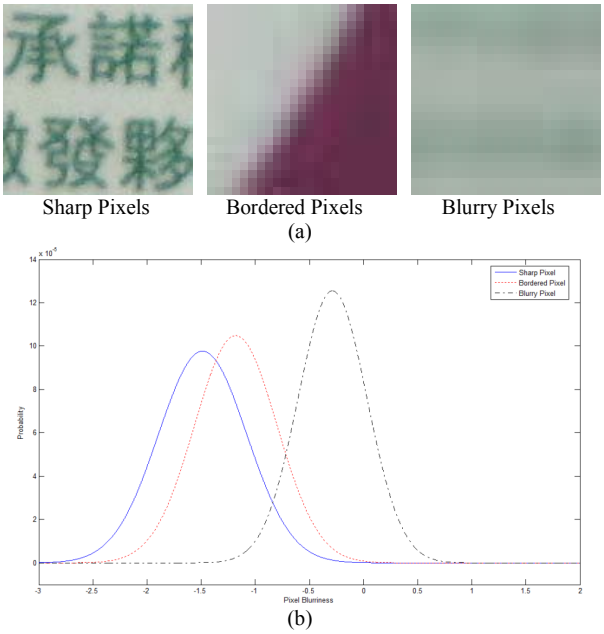

Fig.2. Characteristics of Pixels: (a) the blocks composed of three kinds of pixels, and (b) Gaussian distributions of pixel blurriness for sharp pixel, bordered pixel, and blurry pixel.

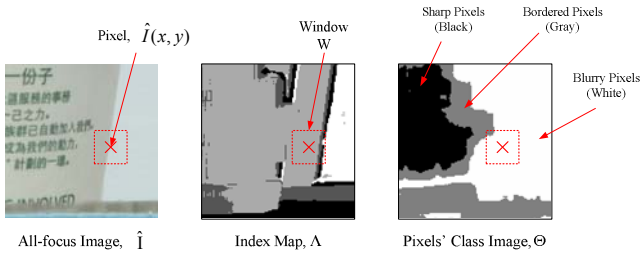

Fig.3. All-focus image ($\hat{\mathrm{I}}$), index map (Λ), pixels' class image (Θ), and window (W). In Θ, the white, gray and black pixels represent blurry pixel, bordered pixel, and sharp pixel.

Step 3. Implementing pixel classification to $\hat{\mathrm{I}}$ by (8) with τ_1 and τ_2, the pixels' class image Θ is acquired.

Step 4. If the (x,y)-th pixel with $\Theta(x,y)$=–1 is identified as sharp pixel, the pixel is kept without replacing.

Step 5. If the (x,y)-th pixel with $\Theta(x,y)$=1 is identified as blurry pixel, the pixel is replaced. Let W be an $L\times L$ window extracted from Λ. The (x,y)-th blurry pixel locates at the center of window as shown in Fig.3. Picking up the blurry pixels within W, the indices of these blurry pixels form a index vector denoted as V, where $\mathrm{V}=\{\lambda_1, \lambda_2, \ldots, \lambda_M\}$. λ_i represents the index of the i-th picked blurry pixel, and M is the number of picked blurry pixels. Subsequently, median filter is applied to V, and the (x,y)-th pixel is replaced according to the following equations,

$$\begin{aligned}&\hat{I}(x,y)=I_{\tilde{k}}(x,y),\\ &\text{where } \tilde{k}=\underset{\mathrm{V}=\{\lambda_1,\lambda_2,\ldots,\lambda_M\}}{MED}(\mathrm{V})\end{aligned} \tag{9}$$

In (9), the function MED(V) outputs the median index of V.

Step 6. The (x,y)-th pixel with $\Theta(x,y)=0$ is identified as bordered pixel. Let W_2 be a window of sized $L'\times L'$ extracted from Λ, and the (x,y)-th bordered pixel locate at the center of W_2. M_S and M_B denote the numbers of sharp pixel and blurry pixel within W_2, respectively. If M_S is larger than or is equal to M_B, the pixel is kept without replacing. Otherwise, the indices of blurry pixels within W_2 form a index vector V', where $V'=\{\lambda_1, \lambda_2, \ldots, \lambda_{M_B}\}$. The replacement criterion to the (x,y)-th bordered pixel is defined as follows,

$$\hat{I}(x,y)=\begin{cases}\hat{I}(x,y) & \text{if } M_S \geq M_B \\ I_{\tilde{k}}(x,y), & \text{otherwise}\end{cases} \qquad (10)$$

where $\tilde{k}=\underset{V'=\{\lambda_1,\lambda_2,\ldots,\lambda_{M_B}\}}{MED}(V')$.

IV. Image Refocusing Method

Sharp and blur effects always appear at real-world photos. In order to realize blur effect with respect to out of focus, Gaussian lowpass filters with different standard deviations are applied to all-focus image. The issue to image refocusing is how to select the proper Gaussian lowpass filters. The proposed image refocusing method is composed of two procedures: establishment of standard deviation-index table and generation of depth-adjustable image. The detail of every procedure is introduced below.

A. Establishment of Standard Deviation-Index Table

The objective of establishing standard deviation-index table is to connect relationship between Gaussian lowpass filter and index. Assuming that an $N\times N$ Gaussian lowpass filter is employed with standard deviation denoted as $\Sigma(d)$, and standard deviation is the function of difference (d) of two image indices. The steps of estimating $\Sigma(d)$ are below.

Step 1. Let $HS(d, \sigma)$ be a histogram value, where d and σ represent index difference and standard deviation, respectively. $\hat{W}(x,y)$ and $W_k(x,y)$ are two $N\times N$ windows extracted from the all-focus image ($\hat{I}$) and the k-th reference image (I_k), respectively. The (x,y)-th pixel locates at the center of window. N_{ref} is the number of reference images.

Step 2. Creating twenty-five Gaussian lowpass filters with the standard deviation σ_i, where $\sigma_i=i\times 0.5$ and $i=\{1, 2, \ldots, 25\}$. $\hat{W}(x,y)$ is operated with those filters, and the proper σ^* of Gaussian lowpass filter is defined as,

$$\sigma^*=\underset{\sigma_i=i\times 0.5}{\arg\min}\left\|\hat{W}(x,y)\otimes\Phi_i - W_k(x,y)\right\|_2^2 \qquad (11)$$

where $k=\{1, 2, \ldots, N_{ref}\}$.

Step 3. The histogram value $HS(d,\sigma)$ is updated by the following equations,

$$HS(d,\sigma)=HS(d,\sigma)+1, \quad \text{where } d=|\Lambda(x,y)-k| \text{ and } \sigma=\sigma^*. \qquad (12)$$

In (12), $\Lambda(x,y)$ denotes the index of the (x,y)-th pixel in $\hat{I}$. The window size is set to 23×23 in all of the experiments. Fig.4 shows a 2D histogram, the horizontal and the vertical axes of histogram represent the index difference and the standard deviation, respectively.

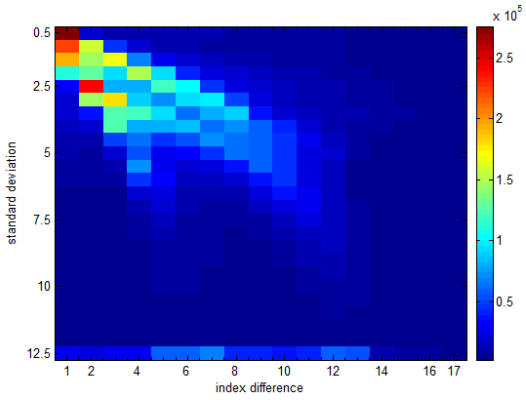

Fig.4. Two-dimensional Histogram

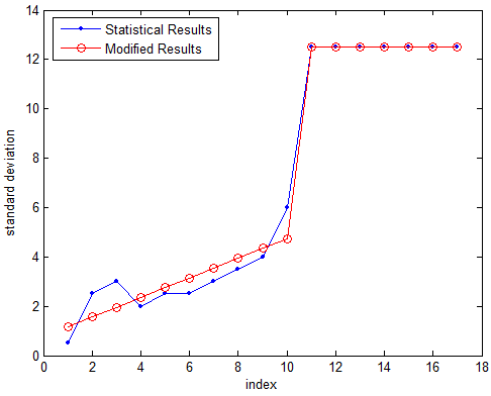

Fig.5. Standard Deviation-Index Curves: The blue curve is the statistical results and the red curve is the modified results. A linear function is approximated to standard deviations at small indices (which is smaller than 11), and standard deviations at large indices is kept without altering.

Step 4. Establishing standard deviation-index table, Σ. First, the $\Sigma(d)$ is found in the 2D histogram according to the following equation,

$$\Sigma(d)=i_d^*\times 0.5, \quad \text{where } i_d^*=\underset{i=\{1,2,\ldots,25\}}{\arg\max}\, HS(d,\sigma_i). \qquad (13)$$

The result of $\Sigma(d)$ estimated by (13) is named the statistical result.

Step 5. Setting a linear function $f(d)$ approximate to standard deviations at small index differences. The standard deviations at large index differences were kept without altering. The modified result of $\Sigma(d)$ is defined by,

$$\hat{\Sigma}(d)=\begin{cases}\Sigma(d) & \text{if } d\geq\tau_d \\ f(d), & \text{otherwise}\end{cases} \qquad (14)$$

where the linear function $f(d)$ is realized by least squares approximation (LSA), and τ_d is a threshold to separate small and large index differences. The result of $\hat{\Sigma}(d)$ is named the modified result.

In the case of Fig.4, there are 18 reference images. The sta-

TABLE I
STANDARD DEVIATION-INDEX TABLE FOR FIG.4

Index Difference d	1	2	3	4	5	6	7	8	9	10	11	12	13	14	15	16	17
Statistical Results $\Sigma(d)$	0.5	2.5	3	2	2.5	2.5	3	3.5	4	6	12.5	12.5	12.5	12.5	12.5	12.5	12.5
Modified Results $\hat{\Sigma}(d)$	1.16	1.56	1.96	2.35	2.75	3.15	3.55	3.94	4.34	4.74	12.5	12.5	12.5	12.5	12.5	12.5	12.5

tistical and modified standard deviation-index tables are listed in the 2nd row and the 3rd row of Table I, and τ_d=11. Fig.5 shows the standard deviation-index curves before and after implementing linear function approximation.

B. Generation of Depth-adjustable Image

Given the target index λ, the proposed refocusing method generates depth-adjustable images from all-focus image $\hat{I}$ by referring to index map and standard deviation-index table. Obviously, index differences of statistical and modified standard deviation-index tables are integers listed in Table I. Once index difference is a non-negative floating-point number, Lagrange's interpolation method is utilized to re-compute the standard deviation-index table which is formulated by,

$$\tilde{\Sigma}(d') = \begin{cases} 0, & \text{if } d' = 0 \\ \sum_{k=1}^{N_{\text{ref}}-1} \left(\prod_{\substack{i=1 \\ i \neq k}}^{N_{\text{ref}}-1} \frac{d' - d_i}{d_k - d_i} \right) \hat{\Sigma}(d_i), & \text{if } d' > 0 \end{cases} \tag{15}$$

where d_i denotes the i-th index difference in Table I. Consequently, the depth-adjustable image $\tilde{I}$ is defined as follows,

$$\tilde{I}(x,y) = \begin{cases} \hat{I}(x,y), & \text{if } \Lambda(x,y) = \lambda \\ J_{|\Lambda(x,y)-D|}(x,y), & \text{otherwise} \end{cases} \tag{16}$$

where $J_{d'} = \hat{I} \otimes \Phi$.

In (16), $J_{d'}(x,y)$ denotes the (x,y)-th pixel value of the filtered all-focus image $\hat{I}$, and Φ is the Gaussian lowpass filter with the standard deviation $\tilde{\Sigma}(d')$.

V. THE EXPERIMENT RESULTS

In this section, we emphasize on three experiments: generations of all-focus image, generation of depth-adjustable image, and the comparisons between our method and the compared approaches. For parameter settings, four Gaussian lowpass filters of sized 23×23 were employed in pixel blurriness measure, and the standard deviations were set to σ_1=0.1, σ_2=5, σ_3=10, and σ_4=20. During pixel classification, two thresholds were τ_1=−0.72 and τ_2=−1.36. The window was sized to 23×23 in image refusing method and τ_d=11 in (14).

A. Generation of All-focus Image

We tested several image sets in the first experiment. One of test image sets included 16 reference images of sized 2048×1536, and the six reference images were shown in Fig.6(a). The in-focus objects in images were the table-tennis ball, the paper cup holder, the paper cup, the lime wall, and the wall of distant building. Finally, the all-focus image was generated by the proposed image fusion method as shown in Fig.6(b). The flower on the left cup is referred to the 4th image, which is sharper than the flowers in the other images. The rest of all-focus images were shown in Website [24].

B. Generation of Depth-adjustable Image

The next experiment concentrated on generation of depth-adjustable image. The all-focus image, index map, and standard deviation-index table were yielded after implementing image fusion method. One of all-focus images had been mentioned in Section IV, which included 18 reference images. The corresponding standard deviation-index table was listed in Table I. Figs.7(a) and 7(b) showed the all-focus image and the corresponding index map, respectively. Implementing the proposed image refocusing method, the three depth-adjustable images were shown in Fig.7(c). The peak signal-to-noise ratio (PSNR) and mean of structure similarity (MSSIM) [25, 26] were computed to assess the difference between the depth-adjustable image and the original reference image. The PSNR curve and MSSIM curve of these 18 depth-adjustable images against different indices were illustrated in Figs.9(a) and 9(b), respectively.

C. Comparisons

In the third experiment, the proposed fusion method was compared with the six existing fusion approaches, including Tian et al.'s approach [12], Haghighat et al.'s two approaches [27], and Naidu et al.'s approaches [4, 5, 6]. In [27], the first approach was performed with variance algorithm in DCT domain, and the second approach was performed with variance algorithm and consistency verification in DCT domain. We were interested in three issues in this experiment: image quality, computational complexity, and artifact. To assess the quality of all-focus image, the average of pixels' blurriness to a whole image was calculated by (3). Computational complexity is an important issue. We calculated time ratio based on the computing time of our method. Once all-focus image has artifact, it means that fusion method generates unnatural result. The comparisons of our method and the six existing approaches were listed in Table II. The all-focus images by using our method and the six existing approaches were shown in Fig.7(a) and Fig.8, respectively. It is obvious that the proposed method generates good-quality all-focus image without artifact. Figs.8(a), 8(d) and 8(e) were blurry, and the artifacts appeared at the logo of Mark cup in Figs.8(b), 8(c), and 8(f). In addition, our method has lower computational complexity than the other ones except Naidu and Raol's approach [4].

Furthermore, we investigated the efficiency of image refocusing by using Gaussian lowpass filter, average filter, and disc filter. The same process to find standard deviation-index table was performed to average filter and disc filter. The

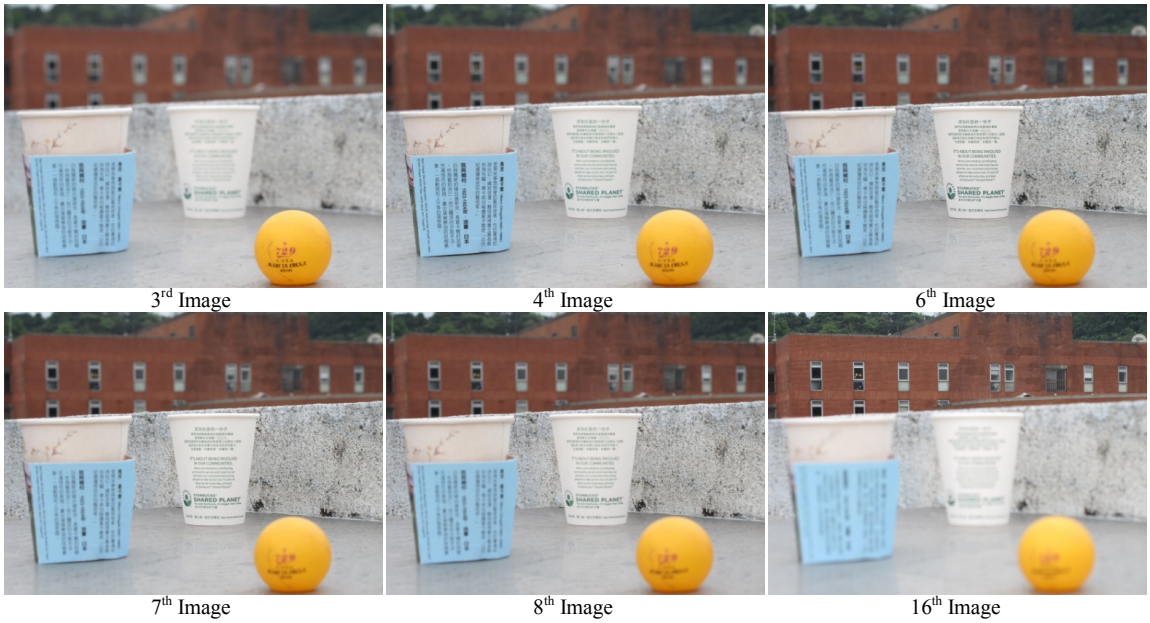

(b)

Fig.6. Results of Image Fusion: (a) the six reference images with different in-focus objects, and (b) the all-focus image

tested image sets included 18 reference images, and the all-focus image was shown in Fig.7(a). Figs.9(a) and 9(b) show the PSNR curves and the MSSIM curves of depth-adjustable images by three filters against different indices. Analyzing the results of Fig.9, both Gaussian lowpass filter and average filter had better quality performances at small indices (correspond to short distances) than disc filter did. At large indices (correspond to long distances), both Gaussian lowpass filter and disc filter had better qualities performances than average filter did. In summary, Gaussian lowpass filter is more stable than average filter and disc filter to generate good-quality depth-adjustable images.

VI. Conclusion

The contributions of this paper are to present image fusion method and image refocusing method to generate all-focus image and depth-adjustable image. The proposed fusion method generates good-quality all-focus image without artifact, and it has low computational complexity. For the proposed refocusing method, we employ Gaussian lowpass filter rather than average filter and disc filter to realize blur effect with

(a)

(b)

Index 5 (PSNR=34.07, MSSIM=0.9096) Index 6 (PSNR=32.91, MSSIM=0.9060) Index 11 (PSNR=35.58, MSSIM=0.9039)

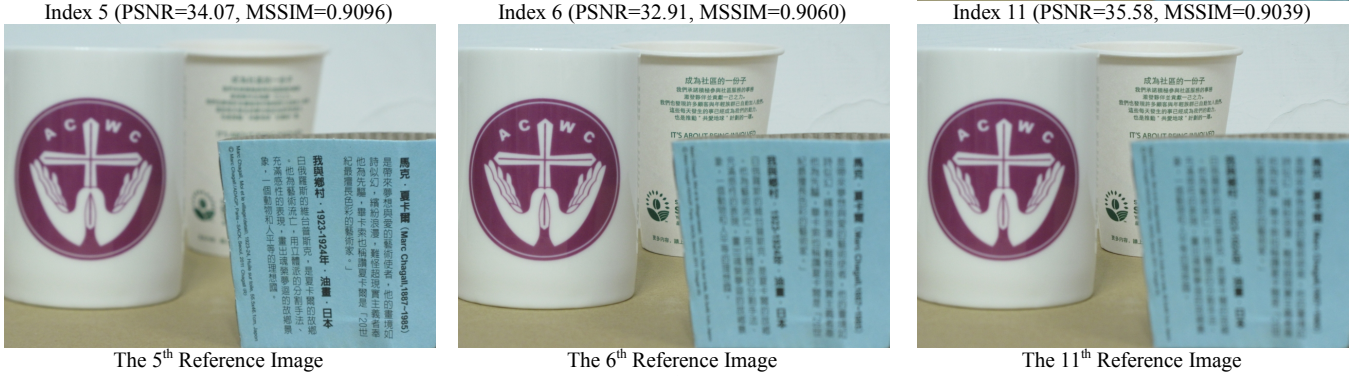

The 5th Reference Image The 6th Reference Image The 11th Reference Image

(c)

Fig.7. Results of Image Refocusing: (a) all-focus image, (b) index map, and (c) three depth-adjustable images and the corresponded reference images.

TABLE II
COMPARISONS OF OUR METHOD AND THE SIX EXISTING APPROACHES

	Our Method	**Tian [12, 30]**	**Haghighat [27, 28]**		**Naidu [4, 29]**	**Naidu [5, 29]**	**Naik M [6, 29]**
Attribution	Pixel	Pixel	DCT	DCT	PCA + Wavelet	SVD	Wavelet
Average of Pixel Blurriness	-0.8976	-0.5689	-0.8960	-0.9408	-0.0735	-0.2737	-0.9353
Time Ratio (second)	1 (15.4)	245.19 (3775.9)	36.26 (558.4)		0.177 (2.73)	6.28 (96.71)	6.80 (104.71)
Artifact			√	√			√
Blurry Image		√			√	√	

respect to out of focus. The experiment result demonstrates that Gaussian lowpass filter is more stable than average filter and disc filter to yield good-quality depth-adjustable image.

REFERENCES

[1] Ren Ng, "Digital light field photography," Stanford Ph.D. Thesis, July 2006.

[2] V. P. S. Naidu, "Multi-resolution image fusion by FFT," *Int'l Conf. on Image Information Processing (ICIIP)*, Shimla India, 3-5 Nov. 2011.

[3] V. P. S. Naidu, "Discrete cosine transform based image fusion techniques," *Journal of Communication, Navigation and Signal Processing*, vol.1, no.1, pp.35-45, Jan. 2012.

[4] V. P. S. Naidu, and J. R. Raol, "Pixel-level image fusion using wavelets and principal component analysis," *Defence Science Journal*, vol.58, no.3, pp.338 -352, May 2008.

(a) Pixel Blurriness=–0.5689 (b) Pixel Blurriness=–0.8960 (c) Pixel Blurriness=–0.9408

(d) Pixel Blurriness=–0.0735 (e) Pixel Blurriness=–0.2737 (f) Pixel Blurriness=–0.9353

Fig.8. All-focus Images by Using Six Existing Fusion Approaches: (a) Tian et al.'s approach [12], (b) Haghighat et al.'s first approach [27], (c) Haghighat et al.'s second approach [27], (d) Naidu and Raol's PCA-Wavelet-based approach [4], (e) Naidu's SVD-based approach [5], and (f) Naik M et al.'s approach [6].

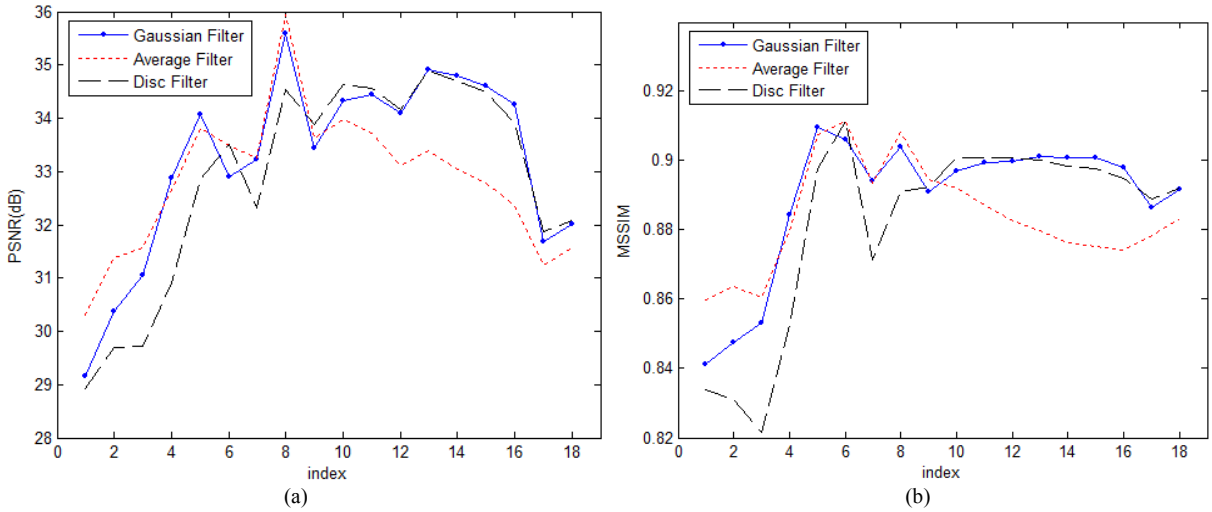

(a) (b)

Fig.9. Qualities of Refocused Depth-adjustable Images by Gaussian Lowpass Filter, Average Filter and Disc Filter: (a) PSNR curves, and (b) MSSIM curves. Gaussian lowpass filter is more stable than average filter and disc filter in image refocusing.

[5] V. P. S. Naidu, "Image fusion technique using multi-resolution singular value decomposition," *Defence Science Journal*, vol.61, no.5, pp.479-484, Sept. 2011.

[6] V. C. Naik M, Shreedarshan, and V. P. S. Naidu, "Pixel- and feature- level image fusion techniques," *National Conf. on Engineering Systems (NACES)*, MSRIT, India, 21-23 Sept. 2011.

[7] S. Li, J. T. Kwok, and Y. Wang, "Multifocus image fusion using artificial neural networks," *Pattern Recognition Letters*, vol.23, pp.985-997, 2002.

[8] W. Huang, and Z. Jing, "Multi-focus image fusion using pulse coupled neural network," *Pattern Recognition Letters*, vol.28, pp.1123-1132, 2007.

[9] X. Qu, and W. Yan, "Multi-focus image fusion algorithm based on regional firing characteristic of pulse coupled neural networks," *BIC-TA*, Zhengzhou, China, pp.62-66, Sept. 2007

[10] R. Maruthi, K. Sankarasubramanian, "Multifocus image fusion based on the information level in the regions of the images," *Journal of Theoretical and Applied Information Technology*, vol.3, no.4, pp.80-85, Dec. 2007.

[11] W. Wang, and F. Chang, "A multi-focus image fusion method based on Laplacian pyramid," *Journal of Computers*, vol.6, no.12, pp.2559-2566, Dec. 2011.

[12] J. Tian, L. Chen, L. Ma and W. Yu, "Multi-focus image fusion

using a bilateral gradient-based sharpness criterion," *Optics Communications*, vol.284, pp.80-87, Jan. 2011.

[13] J. Kong, K. Zheng, J. Zhang, and X. Feng, "Multi-focus image fusion using spatial frequency and genetic algorithm," *Int'l Journal of Computer Science and Network Security*, vol.8, no.2, pp.220-224, Feb. 2008.

[14] H. Li, B. S. Manjunath, and S. K. Mitra, "Multisensor image fusion using the wavelet transform," *Graphical Models and Image Processing*, vol.57, no.3, pp.235-245, May 1995.

[15] X. Yang, W. Yang, and J. Pei, "Different focus points images fusion based on wavelet decomposition," Proc. of the Third *Int'l Conf. on Information Fusion*, vol.1, pp.MOD3/3-MOD3/8, 10-13 July 2000.

[16] F. Luo, B. Lu, and C. Miao, "Multi focus image fusion with trace-based structure tensor," *SPIE 8200, Int'l Conf. on Optical Instruments and Technology: Optoelectronic Imaging and Processing Technology*, Beijing, China, 28 Nov. 2011.

[17] J. Tian, and L. Chen "Adaptive multi-focus image fusion using a wavelet-based statistical sharpness measure," *Signal Processing*, vol.92, No.9, pp.2137-2146, Sept. 2012.

[18] S. Bae, and F. Durand, "Defocus Magnification," *EUROGRAPHICS*, vol.26, no.3, pp.571-579, 2007.

[19] F. Moreno-Noguer, P. N. Belhumeur, and S. K. Nayar, "Active refocusing of images and videos," *ACM Trans. on Graphics, ACM SIGGRAPH*, vol.26, no.3, July 2007.

[20] Y.-C. Zeng, and C.-H. Tsai, "Detection of salient object using pixel blurriness," *APSIPA ASC*, Los Angeles, USA, pp.1-4, Dec. 2012.

[21] J. J. McAnany, M. Shahidi, R. A. Applegate, R. Zelkha, K. R. Alexander, "Contributions of optical and non-optical blur to variation in visual acuity," *Optometry & Vision Science*, vol.88, no.6, pp.716-723, June 2011.

[22] R. O. Duda, P. E. Hart, and D. G. Stork, Pattern classification, John Wiley & Sons Inc., New York, 2001.

[23] S.-C. Pei and Y.-C. Zeng, "Tamper proofing and attack identification of corrupted image by using semi-fragile multiple-watermarking algorithm," *ASIACCS*, Taipei, Taiwan, pp.166-174, March 2006.

[24] Results of Image Fusion and Image Refocusing, https://plus.google.com/109105499373981955157/posts

[25] Z. Wang, A. C. Bovik, H. R. Sheikh and E. P. Simoncelli, "Image quality assessment: from error visibility to structural similarity," *IEEE Trans. Image Processing*, vol.13, no.4, pp.600-612, April 2004.

[26] A. Loza, L. Mihaylova, N. Canagarajah, and D. Bull, "Structural similarity-based object tracking in video sequences," *IEEE Int'l Conf. on Information Fusion*, pp.1-6, July 2006.

[27] M.B.A. Haghighat, A. Aghagolzadeh, and H. Seyedarabi, "Multi-focus image fusion for visual sensor networks in DCT domain," *Computers and Electrical Engineering*, vol.37, no.5, pp.789-797, Sept. 2011.

[28] http://www.mathworks.com/matlabcentral/fileexchange/40861-multi-focus-image-fusion-in-dct-domain

[29] http://www.mathworks.com/matlabcentral/fileexchange/authors/104729

[30] http://www.mathworks.com/matlabcentral/fileexchange/29926-multi-focus-image-fusion-using-a-bilateral-gradient-based-sharpness-criterion